Effects of coherence on temporal resolution

Syamsundar De, Jano Gil-Lopez, Benjamin Brecht, and Christine Silberhorn

Integrated Quantum Optics, Institute for Photonic Quantum Systems (PhoQS), Warburger Straße 100, 33098 Paderborn, Germany

Luis L. Sánchez-Soto

Departamento de Óptica, Facultad de Física, Universidad Complutense, 28040 Madrid, Spain
and Max-Planck-Institut für die Physik des Lichts, Staudtstraße 2, 91058 Erlangen, Germany

Zdeněk Hradil and Jaroslav Řeháček

Department of Optics, Palacký University, 17. listopadu 12, 77146 Olomouc, Czech Republic

Measuring small separations between two optical sources, either in space or in time, constitutes an important metrological challenge as standard intensity-only measurements fail for vanishing separations. Contrarily, it has been established that appropriate coherent mode projections can appraise arbitrarily small separations with quantum-limited precision. However, the question of whether the optical coherence brings any metrological advantage to mode projections is still a point of debate. Here, we elucidate this problem by experimentally investigating the effect of varying coherence on estimating the temporal separation between two single-photon pulses. We show that, for an accurate interpretation, special attention must be paid to properly normalize the quantum Fisher information to account for the strength of the signal.

I. INTRODUCTION

In numerous applications, including radar signal processing [1–3], radio acoustic sounding [4,5], ultrasonic testing [6], and medical imaging [7], one is faced with the challenge of determining the temporal delay between two closely spaced, overlapping, ultrashort pulses. There are several efficient techniques to estimate these small offsets, such as the cross-correlation, phase-shift, and delay line methods [8]. However, all of them conspicuously fail when the time delay is significantly shorter than the pulse duration.

The same pitfall appears in the spatial domain: The resolution of an imaging system is limited by the size of its point spread function (PSF), which specifies the intensity response to a point source [9]. This gives an intuitive picture of the mechanisms that obstruct resolution, but it is very heuristic. For example, the Rayleigh limit [10] is defined as the distance from the center to the first minimum of the PSF. Yet that can be made arbitrarily small with ordinary linear optics, at the price of the sidelobes becoming much higher than the central maximum. This hints that estimating the separation between two points becomes also a matter of photon statistics [11].

Lately, the resolution limits have been revisited from the alternative perspective of quantum metrology. The idea is to use the quantum Fisher information (FI) and the associated quantum Cramér-Rao bound (CRB) to assess how well the separation between two point sources can be estimated [12–17]. For direct imaging, the classical FI drops to zero as the separation between the sources decreases, and the error with which we can determine the separation diverges accordingly, which has been dubbed Rayleigh's curse [18]. Surprisingly, when the quantum FI (i.e., optimized over all measurements allowed by quantum mechanics) is calculated, it stays constant, evidencing that the Rayleigh limit is not essential.

These remarkable predictions have fuelled a number of experimental implementations, both in the spatial [19–22] and the time-frequency [23] domains. The key behind these achievements is the use of phase-sensitive projections onto optimal modes [24] instead of intensity measurements, as the latter discard the phase information carried by the signal.

The approach has been generalized to more realistic scenarios, where the signals may have different intensities. This involves the simultaneous estimation of separation, centroid, and relative intensities [25,26]. Still in this multiparameter case [27–30], optimal quantum-limited measurements have been worked out [31] and experimentally demonstrated [32].

The discussion thus far assumes incoherence between the signals. This conforms with the conditions underlying Rayleigh's criterion. In the temporal domain, this happens with, for example, remote clocks [e.g., the Global Positioning System (GPS)] [33–35], incoherent excitations in biological samples [36], condensed matter physics [37], and astronomical observations [38].

A recent heated debate addressed the role of coherence in the resolution limits [39–46]. Any coherent superposition

of two time-delayed pulses can be decomposed in terms of in-phase and antiphase combinations of the two pulses. Yet, these two channels are not equivalent concerning the strength of the signal: The antiphase mode does carry the information about the temporal separation, but the intensity in this mode vanishes as the time offset decreases. Hence each photon therein carries a huge amount of information.

However, this effect is not necessarily a metrological advantage, because the input signal still contains many photons and thus, on average, the information per photon is limited.

We stress that ignoring the resources required to generate the input signal might lead one to false conclusions about the information content of the measurement. In this sense, the limit of incoherent mixtures represents a bound that cannot be overcome without prior information coded into the state [47]. Coherence may provide extra benefits by sorting information for different parameters into different channels. We confirm here these predictions with an experiment that benefits from classical and quantum resources, both contained in the quantum FI of the signal.

II. THEORETICAL MODEL

Let us first set the stage for our model. To facilitate possible generalizations, we phrase what follows in a quantum language, so that a pulse wave form with complex temporal envelope $\psi(t)$ is assigned to a ket $|\psi\rangle$, such that $\psi(t) = \langle t|\psi\rangle$. Here, we understand that an ideal (sharp) measurement of time would project on the state $|t\rangle$ defined by a delta function in time or, in the frequency representation, by

$$\langle \omega|t\rangle = \frac{1}{\sqrt{2\pi}} e^{i\omega t}. \tag{1}$$

We consider two pulses of identical shape but displaced by a time offset τ, whose magnitude we want to estimate. We define the time-shifted versions, $|\psi_{\pm}\rangle$, as $\psi_{\pm}(t) = \psi(t \pm \tau/2)$. In addition, for convenience, we keep the total intensity normalized to unity:

$$\int_{-\infty}^{\infty} dt \, [|\psi_+(t)|^2 + |\psi_-(t)|^2] = 1. \tag{2}$$

In general, $\langle \psi_-|\psi_+\rangle \neq 0$, so these modes are not orthogonal. This overlap is at the heart of all the difficulties of the problem, for it implies that the two modes cannot be separated by independent measurements.

To capture the essence of the problem, we introduce symmetric and antisymmetric (non-normalized) coherent modes

$$\psi_{\rm s}(t) = \frac{1}{\sqrt{2}} [\psi_+(t) + \psi_-(t)],$$
$$\psi_{\rm a}(t) = \frac{1}{\sqrt{2}} [\psi_+(t) - \psi_-(t)]. \tag{3}$$

These coherent modes can be generated by a mode converter using linear optical transformations. Such an operation is, for instance, readily implemented by sending the two signals into different input ports of a balanced beam splitter. The total intensity is conserved in this process. Physically, the symmetric mode corresponds to an in-phase superposition of

the time-shifted components, whereas the antisymmetric one corresponds to an antiphase superposition.

To proceed further, we need to specify the explicit wave form of the pulse. For simplicity, we will use the standard choice of a Gaussian profile

$$\psi(t) = \frac{1}{(2\pi\sigma_t^2)^{1/4}} \exp\left(-\frac{t^2}{4\sigma_t^2}\right) \tag{4}$$

of width σ_t.

We first consider a fully incoherent mixture of the time-shifted components. Equivalently, this can be prepared as an incoherent sum of the in-phase and anti-phase channels; in the experimental realization this amounts to an equal mixing of the measurement data for each coherent mode in postprocessing. The situation can be thus represented by the following density matrix:

$$\varrho(\tau) = |\psi_+\rangle\langle\psi_+| + |\psi_-\rangle\langle\psi_-| = |\psi_{\rm s}\rangle\langle\psi_{\rm s}| + |\psi_{\rm a}\rangle\langle\psi_{\rm a}|. \tag{5}$$

Now, we can directly apply quantum estimation theory. The pivotal quantity is the quantum FI [48], which is a mathematical measure of the sensitivity of an observable quantity (pulse wave form) to changes in its underlying parameters (time delay). Replicating the calculations performed in the spatial domain [19], one immediately gets that the quantum FI, denoted by $\mathcal{Q}$, is constant, $\mathcal{Q}(\tau) = 1/(4\sigma_t^2)$. The associated quantum CRB ensures then that the variance of any unbiased estimator $\hat{\tau}$ of the time delay τ is lower bounded by the reciprocal of the quantum FI (per single detection event); viz.,

$$\text{Var}_\varrho(\hat{\tau}) \geqslant \frac{1}{\mathcal{Q}(\tau)} = 4\sigma_t^2. \tag{6}$$

In what follows, it will prove convenient to look at the problem from a slightly different perspective. As the optimal measurement attaining the CRB is known, we can calculate the FI for such a measurement. In fact, the optimal scheme involves projections onto the successive derivatives (properly orthonormalized) of the pulse amplitude [24]. For our basic Gaussian wave form, this reduces to the Hermite-Gauss temporal modes

$$\text{HG}_n(t) = \langle t | \text{HG}_n\rangle$$
$$= \frac{1}{(2\pi\sigma_t^2)^{1/4}} \frac{1}{(2^n n!)^{1/2}} H_n\left(\frac{t}{\sqrt{2}\sigma_t}\right) \exp\left(-\frac{t^2}{4\sigma_t^2}\right). \tag{7}$$

Then, we have the following detection probabilities:

$$p_s(n|\tau) \equiv |\langle \text{HG}_n | \psi_{\rm s}\rangle|^2 = \begin{cases} p_n(\tau) & n = 0, 2, 4, \ldots \\ 0 & n = 1, 3, 5, \ldots, \end{cases}$$
$$p_a(n|\tau) \equiv |\langle \text{HG}_n | \psi_{\rm a}\rangle|^2 = \begin{cases} 0 & n = 0, 2, 4, \ldots \\ p_n(\tau) & n = 1, 3, 5, \ldots. \end{cases} \tag{8}$$

Here, $p_\alpha(n|\tau)$ ($\alpha \in \{a, s\}$) denotes the probability density for a detection when projecting the symmetric (antisymmetric) coherent mode $|\psi_{\rm s}\rangle$ ($|\psi_{\rm a}\rangle$) onto the mode HG_n, conditional

on the value of the time delay τ, and we have defined

$$p_n(\tau) = \frac{1}{n! \, 16^n} \left(\frac{\tau}{\sigma_t}\right)^{2n} \exp\left(-\frac{\tau^2}{16\sigma_t^2}\right). \tag{9}$$

Due to the limitations of the experimental setup described later, we cannot generate incoherent signals directly. However, we can generate coherent in-phase and antiphase superpositions, which directly correspond to the output ports of the beam splitter (3). Mixing the measurement data for both superpositions in postprocessing allows for realizing an arbitrary amount of coherence between the two signal pulses.

Note that measuring the output of the interference between two signals is relevant for many applications, such as stellar interferometry, and thus not just a convenient theoretical approach. In consequence, we have now

$$p_{\text{incoh}}(n|\tau) = p_s(n|\tau) + p_a(n|\tau) = p_n(\tau). \tag{10}$$

The classical FI about τ from these mode projections on in-phase and antiphase states is

$$F_{\text{incoh}}(\tau) = \sum_n \frac{1}{p_{\text{incoh}}(n|\tau)} \left[\frac{\partial p_{\text{incoh}}(n|\tau)}{\partial n}\right]^2. \tag{11}$$

Since in-phase and antiphase detection happen in even and odd mode projections, respectively, no information is lost in this process, and the incoherent FI does saturate the quantum bound:

$$F_{\text{incoh}}(\tau) = \frac{1}{4\sigma_t^2}. \tag{12}$$

The incoherent mixture is given either by a sum of time-delayed Gauss components or by a sum of un-normalized in-phase and antiphase superpositions as in (3). The FI for the sum of probabilities in p_{incoh} saturates the ultimate limit for time localization of input components $\psi_\pm$, and the beam splitter action (3) is a unitary process, preserving information. The Hermite-Gauss projections do saturate the quantum bound simultaneously for both in-phase and antiphase superpositions.

Let us now consider the opposite case of fully coherent signals. The estimation of the time shift τ requires projections applied to in-phase and anti-phase states; the results are

$$F_s(\tau) = \frac{1}{8\sigma_t^2} - \left(\frac{1}{8\sigma_t^2} - \frac{\tau^2}{32\sigma_t^4}\right) \exp\left(-\frac{\tau^2}{8\sigma_t^2}\right),$$

$$F_a(\tau) = \frac{1}{8\sigma_t^2} + \left(\frac{1}{8\sigma_t^2} - \frac{\tau^2}{32\sigma_t^4}\right) \exp\left(-\frac{\tau^2}{8\sigma_t^2}\right). \tag{13}$$

If we detect both outputs, we have

$$F_{\text{coh}}(\tau) = \frac{1}{4\sigma_t^2}, \tag{14}$$

which also saturates the quantum bound. Note, though, that for small separations, $\tau \to 0$, we have

$$F_s(\tau) \simeq 0, \quad F_a(\tau) \simeq \frac{1}{4\sigma_t^2}, \tag{15}$$

that is, almost all the information resides in the antiphase channel, F_a. However, in this limit the intensity available in this channel becomes $\sum_n p_a(n|\tau) \to 0$. Nonetheless, we must remember that a constant amount of input intensity is spent

on generating the antiphase superposition for any separation. In a sense, the beam splitter acts as an information sorter that directs the information about the timing separation to the weak antiphase channel. The majority of the signal intensity is sent to the in-phase output, where other parameters (e.g., the timing centroid) can be simultaneously accessed. In the case of complete incoherence, no interference on the beam splitter occurs: The measured intensity in the antiphase output is half of the input intensity, regardless of the timing separation. In this case, a simple intensity measurement is insufficient to resolve the separation of the two signals. It is known, however, that mode projections are ideal and, in fact, remain optimal for any degree of coherence.

A PSF-independent formulation can be provided by defining a modified quantum FI for states with parameter-dependent norm $N(\tau) = \langle\psi(\tau)|\psi(\tau)\rangle$; it reads [47]

$$\widetilde{Q}(\tau) = 4\langle\partial_\tau\psi(\tau)|\partial_\tau\psi(\tau)\rangle + \frac{1}{N(\tau)}[\langle\psi(\tau)|\partial_\tau\psi(\tau)\rangle$$

$$- \langle\partial_\tau\psi(\tau)|\psi(\tau)\rangle]^2. \tag{16}$$

Applying this to the superpositions (3) confirms the optimality of Hermite-Gauss projections.

As we said before, partial coherence has been the subject of a recent controversy [39–44]. Actually, we maintain that partial coherence just redistributes the information into two (or more) interfering channels. Information is carried both by the norm (i.e., intensity modulated by the estimated parameter) and the underlying normalized quantum state. However, total information is preserved and can be extracted with a suitable measurement.

For all degrees of coherence and to remove the impact of an intensity-dependent norm in the experiment, we realize partially coherent states as mixtures of two coherent detection schemes with s and a channels interchanged. We quantify coherence with the parameter γ of such convex combinations, where $\gamma = 0$ means fully coherent and $\gamma = 1/2$ means fully incoherent. The projections on the same temporal Hermite-Gauss modes of in-phase and antiphase channels are

$$P_s^\gamma(n|\tau) = \begin{cases} (1-\gamma)p(n|\tau) & n = 0, 2, 4, \ldots \\ \gamma \, p(n|\tau) & n = 1, 3, 5, \ldots, \end{cases}$$

$$P_a^\gamma(n|\tau) = \begin{cases} \gamma \, p(n|\tau) & n = 0, 2, 4, \ldots \\ (1-\gamma)p(n|\tau) & n = 1, 3, 5, \ldots. \end{cases} \tag{17}$$

Notice that for $\gamma = 1/2$, we obtain two identical sets of probabilities $P_a^{1/2}(n|\tau) = P_s^{1/2}(n|\tau)$, which upon adding we recover the incoherent probabilities $p_{\text{incoh}}(n|\tau)$. Naturally, the total FI again saturates the quantum bound for any γ and all separations

$$F_s^\gamma(\tau) = (1-\gamma)F_s(\tau) + \gamma F_a(\tau),$$

$$F_a^\gamma(\tau) = \gamma F_s(\tau) + (1-\gamma)F_a(\tau), \tag{18}$$

and consequently,

$$F^\gamma(\tau) = F_s^\gamma(\tau) + F_a^\gamma(\tau) = F_{\text{incoh}}(\tau) = \frac{1}{4\sigma_t^2}. \tag{19}$$

From the discussion thus far, it should be clear that Hermite-Gauss temporal modes are optimal for *any* degree of
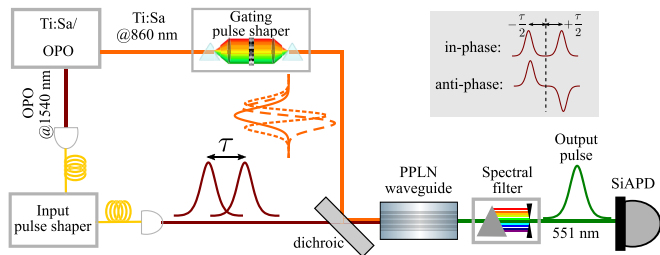
FIG. 1. Schematic of the experimental setup. Inset: In-phase and antiphase input signals. The in-phase and antiphase input pulses with different time shifts τ are derived from a broadband OPO at 1540 nm and attenuated to the few-photon levels using a commercial pulse shaper. Gating pulses at 860 nm with Hermite-Gauss profiles are shaped with an in-house pulse shaper. The input and gating pulses copropagate through a PPLN waveguide. A sum-frequency process generates green output photons at 551 nm which are bandpass filtered and subsequently counted using a silicon avalanche photodiode (SiAPD).

coherence. Of course, any other complete mode decomposition with even or odd temporal symmetry will do the same job [24]. However, these projections require sophisticated equipment. Intensity detection is still the cut-and-dried method used in the laboratory. As the dominant part of the information about separation is contained in the norm of the antiphase superposition, total intensity represents a valuable source of information.

For incoherent states, intensity detection leads to Rayleigh's curse, and it is not optimal. For full coherence, however, intensity detection is one optimal solution. This can be readily shown by calculating the FI for the intensity profiles of in-phase and antiphase channels, whose probabilities of detection are $P_\alpha(t|\tau) = |\psi_\alpha(t)|^2$, with $\alpha \in \{a, s\}$, whence we get

$$F_\alpha^{\mathrm{int}}(\tau) = \int dt \frac{1}{P_\alpha(t|\tau)} \left[\frac{\partial P_\alpha(t|\tau)}{\partial \tau} \right]^2 = F_\alpha(\tau), \quad (20)$$

with $F_\alpha(\tau)$ given by (13). Therefore $F_s^{\mathrm{int}}(\tau) + F_a^{\mathrm{int}}(\tau) = 1/\sigma_t$, and there is no need for sophisticated mode projections when working with a fully coherent signal. However, the temporal resolution can be strongly improved by these detections for partially coherent and incoherent signals, especially in the limit $\tau \to 0$, which is precisely the regime of interest.

III. EXPERIMENTAL RESULTS

The key building block in our experiment for the implementation of the optimal Hermite-Gauss temporal-mode projections is a quantum pulse gate (QPG) [49,50]. It is based on group-velocity matched sum-frequency generation between a strong gating pulse and a weak signal pulse in a nonlinear waveguide. Detecting the upconverted photons then realizes projective measurements, in which the temporal-mode projections are defined by the shapes of the gating pulse.

The detailed scheme of our experimental setup is sketched in Fig. 1. A titanium-sapphire (Ti:Sa) laser and an optical parametric oscillator (OPO) provide the gating and the input pulses with a repetition rate of 80 MHz, respectively. The gating pulses are carved from a laser spectrum centered at 860 nm with a full width at half maximum

(FWHM) bandwidth of 7.25 nm. The gating pulses are shaped into user-defined Hermite-Gauss temporal modes with a home-built pulse shaper, composed of a spatial light modulator at the Fourier plane of a $4f$ line arrangement.

The input pulses are derived from the OPO, delivering light at 1540 nm with an FWHM bandwidth of 23 nm. A commercial fiber-coupled pulse shaper prepares the input signal that consists of coherent superpositions of two time-shifted Gaussian pulses of 1.26 ps width with equal (in-phase) or opposite (antiphase) phase. As shown in the inset of Fig. 1, one receives a positive time shift of $\tau/2$, and the other one receives a negative time shift of $-\tau/2$ with respect to a reference that is set at zero without loss of generality. In our experiment, seven different time shifts ranging from 0 to σ_τ are realized for both in-phase and antiphase inputs by programming the pulse shaper. Moreover, the input pulses are attenuated to a few photons per pulse.

The shaped gating and the input pulses are combined on a dichroic mirror and then coupled into a home-built QPG—a 3.5-cm-long periodically poled lithium niobate (PPLN) waveguide with a poling period of 4.4 μm. The waveguide is designed for spatially single-mode propagation of the input signal, whereas the propagation of the gating beam in the fundamental spatial mode is ensured via optical mode matching. The sum-frequency process yields a green output at 551 nm that undergoes tight spectral filtering in a $4f$ line to discard the phase-matching sidelobes, resulting in an FWHM bandwidth of 40 pm. The filtered output is detected with a fiber-coupled silicon avalanche photodiode (SiAPD). Finally, we record the single counts using a commercial time tagger. We record data for 16 ms for each setting of the input and gating pulses and repeat the measurement 100 times for the statistical analysis of the data.

In our experiment, different coherence strengths are achieved in postprocessing by controlled mixing of the measured data for the in-phase and the antiphase input signals: Each of them separately corresponds to the fully coherent case; their equal mixing leads to the incoherent case, and unequal mixing corresponds to the partial coherence. Rather than using the theoretical projections, we determine the actual input-output relations of the implemented imperfect QPG device, enabling the construction of an unbiased estimator of the time separation despite the limited selectivity of the device [23].

For each coherence setting, this is achieved by fitting the average responses of the first four Hermite-Gauss projections with fourth-order polynomials in τ. The resulting measurement matrix is then used to process the individual detections taking the generalized least-squares estimator constrained by the condition $\hat{\tau} \geq 0$. Estimator statistics are calculated from 100 repeated measurements for each combination of τ and γ parameters.

We had to take special care to avoid unwanted temporal drift between the signal and gating fields that mainly originates from thermal fluctuations. To remove the effect of residual drift, the two fields are recentered by software control after every ten measurement runs of each setting.

Figure 2 shows the statistics of the experimental estimates of τ for incoherent, coherent, and partially coherent superpositions. Mean values are plotted with standard devi-
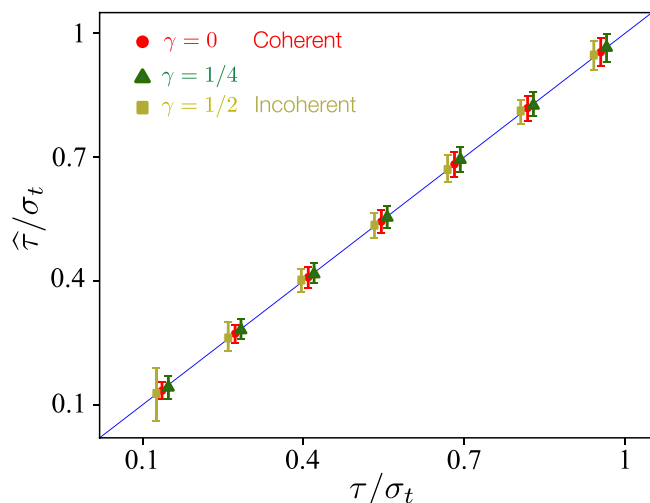
FIG. 2. Estimates $\widehat{\tau}$ vs true separations τ, both in units of the pulse width σ_t for the three values of the coherence indicated in the key.

FIG. 4. Estimation errors for fully coherent signal ($\gamma = 0$) per single total detection (purple circles, as in Fig. 3) and per single antisymmetric (ψ_a) detection (brown squares). The quantum (red solid line) and classical incoherent (blue dashed line) limits are also shown.

ation bars. The true values are inside the standard deviation intervals for all separations, and the estimator bias is negligible.

Figure 3 shows the estimation errors (quantified by the variance) for five different mixtures ranging from fully coherent to incoherent. Coherent estimates saturate the quantum bound for small separations: We experimentally resolve temporal offsets ten times smaller than their pulse duration, with a tenfold improvement in precision over the intensity-only CRB. When coherence is reduced, we see an increase in the experimentally determined variances, especially for the smallest measured time separations. This effect is a consequence
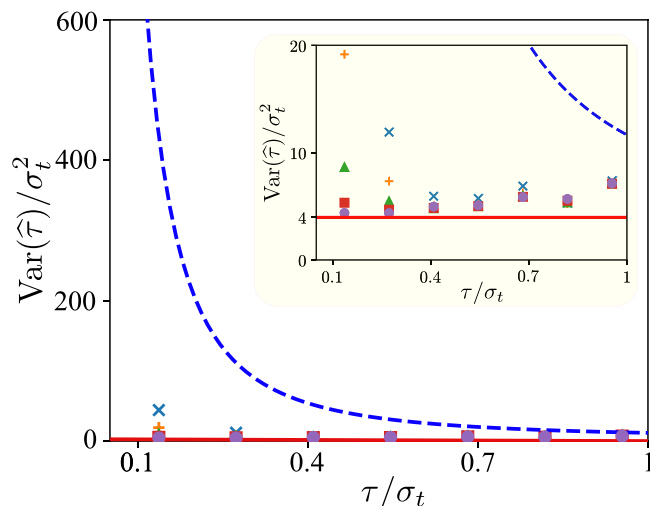
of a tiny, yet non-negligible, cross talk between the odd and even Hermite-Gauss projections. Leakage of the strongly populated HG_0 mode of the symmetric channel towards odd projections, upon mixing the channels as in (17), degrades the information carried by the weaker odd modes (and, in particular, the mode HG_1) of the antisymmetric channel. However, even with these imperfections, we are still much below the intensity-only CRB.

Finally, in Fig. 4 we show the same errors for fully coherent superposition both per single total detection and per single detection in the antisymmetric (ψ_a) channel. The information carried by one such copy seemingly diverges at $\tau \to 0$ and violates the incoherent quantum CRB (QCRLB) (brown squares). However, a proper resource counting, in this case the total single counts, leads to the correct quantum-limited estimation error (purple circles). This is another way of expressing our previous statement that coherence acts as an information sorter condensing information about separation in the *dark* antisymmetric channel.

FIG. 3. Variance of the estimator $\widehat{\tau}$ as a function of the true time offset τ for several values of the coherence parameter γ: 1/2 (blue crosses), 3/8 (orange pluses), 1/4 (green triangles), 1/8 (red squares), and 0 (purple circles). The ultimate limit given by the quantum CRB is given by the red solid line, whereas the classical incoherent detection limit is the dashed blue line. The inset shows a zoomed-in version where we can better appreciate the behavior.
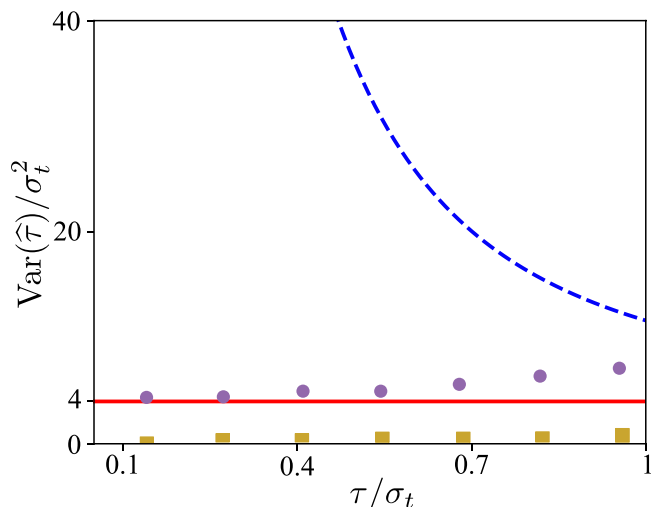
IV. CONCLUDING REMARKS

By resorting to mode-selective measurements, sub-pulse-width separations can be estimated with quantum-limited precision for a full range of temporal coherence. Seemingly, coherence by itself does not provide a direct metrological advantage in time resolution; incoherent superpositions set the ultimate limits in all cases.

However, we stress that coherence can be exploited as an information sorter, distributing information about different parameters into different channels. In our case, for small-time delays, all information is accessible from vanishing intensity in the antisymmetric channel while the bulk of the intensity goes into the symmetric channel, left available for measurements of other relevant physical parameters.

ACKNOWLEDGMENTS

[1] D. Orlando, C. Hao, A. Aubry, G. Cui, A. C. Gurbuz, and S. Gazor, Special issue: Advanced techniques for radar signal processing, EURASIP J. Adv. Signal Process. **2017**, 47 (2017).

[2] S. H. Javadi and A. Farina, Radar networks: A review of features and challenges, Inf. Fusion **61**, 48 (2020).

[3] F. Gini, Grand challenges in radar signal processing, Front. Signal Process. **1**, 664232 (2021).

[4] G. Peters, H. Timmermann, and H. Hinzpeter, Temperature sounding in the planetary boundary layer by RASS—system analysis and results, Int. J. Remote Sens. **4**, 49 (1983).

[5] N. Matuura, Y. Masuda, H. Inuki, S. Kato, S. Fukao, T. Sato, and T. Tsuda, Radio acoustic measurement of temperature profile in the troposphere and stratosphere, Nature (London) **323**, 426 (1986).

[6] C. L. de Korte, A. F. W. van der Steen, B. H. J. Dijkman, and C. T. Lancée, Performance of time delay estimation methods for small time shifts in ultrasonic signals, Ultrasonics **35**, 263 (1997).

[7] W. Drexler and J. G. Fujimoto, *Optical Coherence Tomography* (Springer, Berlin, 2008).

[8] K. Dudáček, *Short Time Delay Measurement*, Tech. Rep. DCSE/TR-2015-03, University of West Bohemia, Pilsen (2015).

[9] J. W. Goodman, *Introduction to Fourier Optics* (Roberts, Englewood, 2004).

[10] Lord Rayleigh, Investigations in optics, with special reference to the spectroscope, Philos. Mag. **8**, 261 (1879).

[11] L. Schermelleh, R. Heintzmann, and H. Leonhardt, A guide to super-resolution fluorescence microscopy, J. Cell Biol. **190**, 165 (2010).

[12] M. Tsang, R. Nair, and X.-M. Lu, Quantum Theory of Superresolution for Two Incoherent Optical Point Sources, Phys. Rev. X **6**, 031033 (2016).

[13] R. Nair and M. Tsang, Far-Field Superresolution of Thermal Electromagnetic Sources at the Quantum Limit, Phys. Rev. Lett. **117**, 190801 (2016).

[14] C. Lupo and S. Pirandola, Ultimate Precision Bound of Quantum and Subwavelength Imaging, Phys. Rev. Lett. **117**, 190802 (2016).

[15] M. Tsang, Subdiffraction incoherent optical imaging via spatial-mode demultiplexing, New J. Phys. **19**, 023054 (2017).

[16] S. Zhou and L. Jiang, Modern description of Rayleigh's criterion, Phys. Rev. A **99**, 013808 (2019).

[17] L. Peng and X.-M. Lu, Generalization of Rayleigh's criterion on parameter estimation with incoherent sources, Phys. Rev. A **103**, 042601 (2021).

[18] M. Tsang, Resolving starlight: A quantum perspective, Contemp. Phys. **60**, 279 (2019).

[19] M. Paúr, B. Stoklasa, Z. Hradil, L. L. Sánchez-Soto, and J. Řeháček, Achieving the ultimate optical resolution, Optica **3**, 1144 (2016).

[20] F. Yang, A. Taschilina, E. S. Moiseev, C. Simon, and A. I. Lvovsky, Far-field linear optical superresolution via heterodyne detection in a higher-order local oscillator mode, Optica **3**, 1148 (2016).

[21] W.-K. Tham, H. Ferretti, and A. M. Steinberg, Beating Rayleigh's Curse by Imaging Using Phase Information, Phys. Rev. Lett. **118**, 070801 (2017).

[22] F. Yang, R. Nair, M. Tsang, C. Simon, and A. I. Lvovsky, Fisher information for far-field linear optical superresolution via homodyne or heterodyne detection in a higher-order local oscillator mode, Phys. Rev. A **96**, 063829 (2017).

[23] J. M. Donohue, V. Ansari, J. Řeháček, Z. Hradil, B. Stoklasa, M. Paúr, L. L. Sánchez-Soto, and C. Silberhorn, Quantum-Limited Time-Frequency Estimation through Mode-Selective Photon Measurement, Phys. Rev. Lett. **121**, 090501 (2018).

[24] J. Řeháček, M. Paúr, B. Stoklasa, Z. Hradil, and L. Sánchez-Soto, Optimal measurements for resolution beyond the Rayleigh limit, Opt. Lett. **42**, 231 (2017).

[25] J. Řeháček, Z. Hradil, B. Stoklasa, M. Paúr, J. Grover, A. Krzic, and L. L. Sánchez-Soto, Multiparameter quantum metrology of incoherent point sources: Towards realistic superresolution, Phys. Rev. A **96**, 062107 (2017).

[26] A. Chrostowski, R. Demkowicz-Dobrzański, M. Jarzyna, and K. Banaszek, On superresolution imaging as a multiparameter estimation problem, Int. J. Quantum Inf. **15**, 1740005 (2017).

[27] S. Ragy, M. Jarzyna, and R. Demkowicz-Dobrzański, Compatibility in multiparameter quantum metrology, Phys. Rev. A **94**, 052108 (2016).

[28] M. Szczykulska, T. Baumgratz, and A. Datta, Multi-parameter quantum metrology, Adv. Phys. X **1**, 621 (2016).

[29] F. Albarelli, M. Barbieri, M. G. Genoni, and I. Gianani, A perspective on multiparameter quantum metrology: From theoretical tools to applications in quantum imaging, Phys. Lett. A **384**, 126311 (2020).

[30] J. S. Sidhu and P. Kok, Geometric perspective on quantum parameter estimation, AVS Quantum Sci. **2**, 014701 (2020).

[31] J. Řeháček, Z. Hradil, D. Koutný, J. Grover, A. Krzic, and L. L. Sánchez-Soto, Optimal measurements for quantum spatial superresolution, Phys. Rev. A **98**, 012103 (2018).

[32] V. Ansari, B. Brecht, J. Gil-Lopez, J. M. Donohue, J. Řeháček, Z. Hradil, L. L. Sánchez-Soto, and C. Silberhorn, Achieving the ultimate quantum timing resolution, PRX Quantum **2**, 010301 (2021).

[33] F. R. Giorgetta, W. C. Swann, L. C. Sinclair, E. Baumann, I. Coddington, and N. R. Newbury, Optical two-way time and frequency transfer over free space, Nat. Photonics **7**, 434 (2013).

[34] W. Gao, S. W. Kim, H. Bosse, H. Haitjema, Y. L. Chen, X. D. Lu, W. Knapp, A. Weckenmann, W. T. Estler, and H. Kunzmann, Measurement technologies for precision positioning, CIRP Ann. **64**, 773 (2015).

[35] W. Kim, J. Jang, S. Han, S. Kim, J. S. Oh, B. S. Kim, Y.-J. Kim, and S.-W. Kim, Absolute laser ranging by time-of-flight measurement of ultrashort light pulses, J. Opt. Soc. Am. A **37**, B27 (2020).

[36] B. Chen, T. Chakraborty, S. Daetwyler, J. D. Manton, K. Dean, and R. Fiolka, Extended depth of focus multiphoton microscopy via incoherent pulse splitting, Biomed. Opt. Express **11**, 3830 (2020).

[37] F. Krausz and M. Ivanov, Attosecond physics, Rev. Mod. Phys. **81**, 163 (2009).

[38] P. Krehlik, Ł. Buczek, J. Kołodziej, M. Lipiński, Ł. Śliwczyński, J. Nawrocki, P. Nogaś, A. Marecki, E. Pazderski, P. Ablewski, M. Bober, R. Ciuryło, A. Cygan, D. Lisak, P. Masłowski, P. Morzyński, M. Zawada, R. M. Campbell, J. Pieczerak, A. Binczewski *et al.*, Fibre-optic delivery of time and frequency to VLBI station, Astron. Astrophys. **603**, A48 (2017).

[39] W. Larson and B. E. A. Saleh, Resurgence of Rayleigh's curse in the presence of partial coherence, Optica **5**, 1382 (2018).

[40] M. Tsang and R. Nair, Resurgence of Rayleigh's curse in the presence of partial coherence: Comment, Optica **6**, 400 (2019).

[41] W. Larson and B. E. A. Saleh, Resurgence of Rayleigh's curse in the presence of partial coherence: Reply, Optica **6**, 402 (2019).

[42] Z. Hradil, J. Řeháček, L. Sánchez-Soto, and B.-G. Englert, Quantum Fisher information with coherence, Optica **6**, 1437 (2019).

[43] K. Liang, S. A. Wadood, and A. N. Vamivakas, Coherence effects on estimating two-point separation, Optica **8**, 243 (2020).

[44] S. A. Wadood, Y. Zhou, J. Yang, K. Liang, M. A. Alonso, X.-F. Qian, T. M. S. M. H. Rafsanjani, A. N. Jordan, R. W. Boyd, and A. N. Vamivakas, Superresolution of partially coherent light sources using parity sorting, Opt. Express **29**, 22034 (2021).

[45] M. Tsang, Poisson quantum information, arXiv:2103.08532.

[46] K. Liang, S. A. Wadood, and N. Vamivakas, Coherence effects on estimating general sub-Rayleigh object distribution moments, arXiv:2105.06817.

[47] Z. Hradil, D. Koutny, and J. Řeháček, Exploring the ultimate limits: Super-resolution enhanced by partial coherence, Opt. Lett. **46**, 1728 (2021).

[48] C. W. Helstrom, *Quantum Detection and Estimation Theory* (Academic, New York, 1976).

[49] A. Eckstein, B. Brecht, and C. Silberhorn, A quantum pulse gate based on spectrally engineered sum frequency generation, Opt. Express **19**, 13770 (2011).

[50] B. Brecht, A. Eckstein, R. Ricken, V. Quiring, H. Suche, L. Sansoni, and C. Silberhorn, Demonstration of coherent time-frequency Schmidt mode selection using dispersion-engineered frequency conversion, Phys. Rev. A **90**, 030302(R) (2014).